

Nematicity and quantum paramagnetism in FeSe

Fa Wang,^{1,2} Steven A. Kivelson,³ and Dung-Hai Lee^{4,5}

¹*International Center for Quantum Materials,*

School of Physics, Peking University, Beijing 100871, China.

²*Collaborative Innovation Center of Quantum Matter, Beijing, China.*

³*Department of Physics, Stanford University, Stanford, California 94305, USA.*

⁴*Department of Physics, University of California, Berkeley, CA 94720, USA.*

⁵*Materials Sciences Division, Lawrence Berkeley*

National Laboratory, Berkeley, CA 94720, USA.

Abstract

In common with other iron-based high temperature superconductors, FeSe exhibits a transition to a “nematic” phase below 90 Kelvin in which the crystal rotation symmetry is spontaneously broken. However, the absence of strong low-frequency magnetic fluctuations near or above the transition has been interpreted as implying the primacy of orbital ordering. In contrast, we establish that quantum fluctuations of spin-1 local moments with strongly frustrated exchange interactions can lead to a nematic quantum paramagnetic phase consistent with the observations in FeSe. We show that this phase is a fundamental expression of the existence of a Berry’s phase associated with the topological defects of a Néel antiferromagnet, in a manner analogous to that which gives rise to valence bond crystal order for spin 1/2 systems. We present an exactly solvable model realizing the nematic quantum paramagnetic phase, discuss its relation with the spin-1 $J_1 - J_2$ model, and construct a field theory of the Landau-forbidden transition between the Néel state and this nematic quantum paramagnet.

Insulating quantum paramagnets (PM) are magnetic systems with only short-range antiferromagnetic (AF) correlations even at zero temperature. Examples of quantum paramagnetic states include valence bond solids (VBS), symmetry protected topological states (SPTs), and spin liquids. Interest in quantum paramagnets was greatly intensified following the proposal¹ (since shown to be incorrect) that the parent insulator of the cuprate high temperature superconductors (HTSC) might be a spin liquid. Because of the proposed relevance to the cuprates, special attention has been paid to square lattice $S = 1/2$ systems, and in particular to the $J_1 - J_2$ Heisenberg model,

$$H = J_1 \sum_{\langle ij \rangle} \mathbf{S}_i \cdot \mathbf{S}_j + J_2 \sum_{\langle\langle jk \rangle\rangle} \mathbf{S}_j \cdot \mathbf{S}_k. \quad (1)$$

where $\langle ij \rangle$ and $\langle\langle jk \rangle\rangle$ denote nearest-neighbor (NN) and second neighbor pairs of sites. Numerical studies have shown²⁻⁴ that the ground state of equation (1) has Néel AF order for $0 \leq J_2/J_1 \lesssim 0.4$ and stripe AF order [see Fig. 2(a,b)] for $0.6 \lesssim J_2/J_1$. Both these phases have gapless $S = 1$ (spin wave) excitations. For $0.4 \lesssim J_2/J_1 \lesssim 0.6$ the ground state appears to have no magnetic order. However, there remain important unresolved issues concerning the precise character of this phase or phases; at least for $0.5 \lesssim J_2/J_1 \lesssim 0.6$ there is fairly compelling evidence of translation symmetry breaking VBS order with an energy gap for spin-1 excitations.

The curious fact that upon restoring the spin rotation symmetry the breaking of spatial translation symmetry follows rests on a uniquely quantum mechanical effect associated with the Berry's phase of the monopole events.^{5,6} A monopole (anti-monopole) is a space-time event [see Fig. 1(a)] across which the “skyrmion number” (see the caption of Fig. 1) changes by $+1(-1)$. The proliferation of monopoles randomizes the Néel order parameter hence causes the system to become a PM. In Ref.⁵, it was argued that monopole events contribute to the path integral with a phase factor that depends on the monopole's spatial location [see Fig. 1(b,c)].

Spin models based on local moments, such as the $J_1 - J_2$ model, have found renewed applications in the young field of iron-based superconductivity. The iron-based HTSCs have layers of Fe^{2+} ions which form a square lattice at high temperatures. Many experimental and theoretical studies have concluded that, with the possible exception of heavily phosphorous

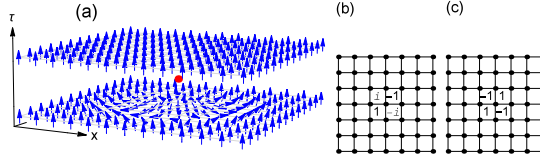


FIG. 1: **The monopole phase factors.** A monopole is a singular configuration of the Néel order parameter whose direction is depicted by an unit vector \hat{n} at each point in space and time. The Néel order parameter configurations before and after a monopole event differ topologically – the skyrmion number changes by one. To understand the skyrmion number imagine assigning an unit vector to each point of a two dimensional space subject to periodic boundary conditions. Such an assignment is a “map” from a torus to the unit sphere S^2 . These maps can be grouped into topological classes, where only maps within the same class can be smoothly deformed into one another. An integer, namely the number of times, and sense, the image of the torus wrap around the unit sphere, characterizes each class. The skyrmion number is given by $q_s = \frac{1}{4\pi} \int dx dy \hat{n} \cdot \partial_x \hat{n} \times \partial_y \hat{n}$. A close inspection of the arrow patterns in panel (a) reveal that before the monopole event (marked by the red dot), the skyrmion number is -1 , while that after the monopole event it is 0 . An analogous figure can be drawn for an anti-monopole across which the skyrmion number jumps by -1 . Haldane showed that associated with each charge q_m monopole event there is a phase factor, $\eta_{\mathcal{R}}^{q_m}$, which enters the path integral over all possible \hat{n} configurations in space and (imaginary) time⁵. This phase factor depends on the spatial location of the monopole core, which it is natural to associate with the center of a lattice plaquette, \mathcal{R} . There is some arbitrariness in the choice of $\eta_{\mathcal{R}}$, but a consistent pattern for spin-1/2 on a square lattice is shown in panel (b) and for spin-1 in panel (c).

doped members of the 122 family, the electronic correlations in the iron-based materials, in particular in the iron chalcogenides, are strong⁷⁻⁹. Moreover, relatively large local magnetic moments in many of these materials have been inferred¹⁰. For FeSe the itinerant electrons only give rise to tiny Fermi pockets¹¹⁻¹⁴. Thus, it is plausible that the magnetism of FeSe can be addressed using a spin model as a starting point.

For many iron-based materials, depending on the doping level, there is “stripe” AF order at low temperatures [see Fig. 2(a,b)]. Due to the breaking of crystal rotation symmetry the stripe order is accompanied by a tetragonal to orthorhombic lattice distortion. In some cases,

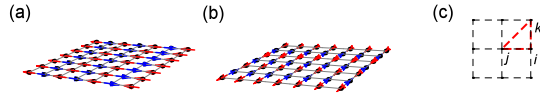


FIG. 2: **The stripe AF and the interactions in H_K** : Panels (a) and (b) show two degenerate versions of a stripe AF ground state corresponding to the two possible directions of the ordering vector, where the arrows schematically represent the ordered magnetic moments on the Fe sites. Panel (c) illustrates the three-site interaction corresponding to each individual projection operator from equation (2).

e.g. in electron-doped Ba-122 materials, the lattice distortion can exist without stripe order [see Fig. 3(a)]. In Ref.¹⁵ it was shown that the distortion is driven by electronic nematicity rather than a lattice (phonon) instability. It has been argued that such nematicity reflects an underlying stripe ordering tendency, and the reason it can exist without the magnetic order is because thermal fluctuations of the continuously varying spin orientation are more severe than of the discrete nematic director^{16–18}.

A potential problem with this perspective is the thermal evolution observed in FeSe crystals, in which nematicity onsets at $T_{\text{nem}} \sim 90\text{K}$, but there is no magnetic ordering down to the lowest measured temperatures suggesting the possibility of a zero temperature nematic quantum PM phase [Fig. 3(b)]. This fact coupled with the absence of any observed enhancement of the low frequency magnetic fluctuations at T_{nem} ^{19,20} has led many to conclude that the nematicity in FeSe is driven by orbital ordering.

Certainly, it is clear that within a local moment picture the lack of magnetic order implies that the spin-spin interactions must be highly frustrated; this is true regardless of what causes the nematic ordering. Thus in the following we ask, “Can frustrated spin interactions alone drive a nematic quantum PM state?”

We consider models in which each Fe^{2+} possesses a localized spin 1 (*e.g.* the $S = 1$ version of the model in equation (1)). Given the strength of Hund’s coupling and the crystal-field splittings, $S = 1$ is a reasonable possibility for the spin of Fe^{2+} ions. However it is important to keep in mind that FeSe is not an insulator, and such localized models neglect the effects of itinerant carriers. We shall return to this point later.

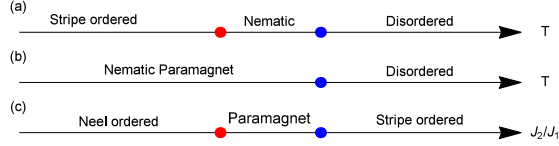


FIG. 3: **Schematic phase diagrams:** (a) The thermal phase diagram of many iron-based superconducting materials. The blue and red dots represent two distinct phase transitions: as a function of decreasing T , the discrete crystal rotation symmetry is spontaneously broken at the blue point and continuous spin rotation symmetry at the red. (b) A likely thermal phase diagram of FeSe. (c) The zero temperature phase diagram of the spin-1 J_1 - J_2 model in equation (1) as a function of J_2/J_1 .

First we demonstrate the existence of a nematic quantum PM phase in an exactly solvable Hamiltonian. Consider a square lattice of $S = 1$ spins interacting via the short-range, spin rotationally invariant Hamiltonian

$$H_K = K \sum_{\langle ij k \rangle} P_3(\mathbf{S}_i + \mathbf{S}_j + \mathbf{S}_k), \quad (2)$$

where $K > 0$ and $\sum_{\langle ij k \rangle}$ sums over all elementary triangles of sites [see Fig. 2(c)], and where \overline{ji} and \overline{ik} are NN bonds and \overline{jk} is a next-NN bond. Here $P_3(\mathbf{S}) = (1/720)S^2(S^2 - 2)(S^2 - 6)$ is the projection operator onto $S = 3$. We note that because it involves spin-1 operators, equation (2) possesses a global spin $\text{SO}(3)$ [rather than $\text{SU}(2)$] symmetry. In addition it possesses all crystalline symmetries of the square lattice (*i.e.* translation and point group symmetries). Moreover, there are two degenerate ground states which can be constructed exactly as follows: Any closed loop $\mathcal{C}_{i_1, \dots, i_n}$ on the lattice can be thought of as a spin-1 chain. The famous AKLT (Affleck-Kennedy-Lieb-Tasaki) state²¹ of such chains can be written as the matrix product state $|\mathcal{C}_{i_1, \dots, i_n}\rangle = \sum_{m_{i_1}=-1}^1 \dots \sum_{m_{i_n}=-1}^1 \text{Tr}[A(m_{i_1}) \dots A(m_{i_n})] |m_{i_1}, \dots, m_{i_n}\rangle$, where $m_{i_k} = -1, 0, 1$ is the S_z quantum number of the spin on site i_k , and the matrices $A(m)$ are $A(\pm 1) = (i\sigma_y \mp 1)/2\sqrt{2}$, $A(0) = \sigma_z/2$, with $\sigma_{y,z}$ being the Pauli matrices. We identify the two adjacent sites i_k and i_{k+1} in an AKLT loop as an ‘‘AKLT-entangled pair’’, and graphically represent it by a blue bond connecting i_k and i_{k+1} in Fig. 4. The two ground-states of H_K are constructed as the direct product of AKLT loop states on all the loops made by connecting nearest-neighbor sites in the x direction, $|X\rangle = \prod_{y=1}^N |\mathcal{C}_{(1,y), (2,y), \dots, (N,y)}\rangle$,

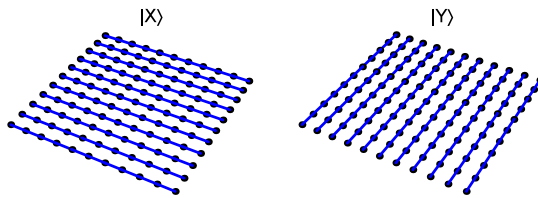


FIG. 4: **The nematic paramagnetic ground states of H_K from equation (2).** The solid blue lines connect AKLT-entangled pairs discussed in the main text.

or in the y direction, $|Y\rangle = \prod_{x=1}^N |\mathcal{C}_{(x,1),(x,2),\dots,(x,N)}\rangle$, where (x, y) with $x, y = 1, \dots, N$ labels the sites of a $N \times N$ square lattice. The graphical representations of $|X\rangle$ and $|Y\rangle$ are shown in Fig. 4. Because the maximum total spin of an AKLT-entangled pair is $S = 1$ ²¹, it follows that the maximum spin component of a triplet of spins $\langle ijk \rangle$ containing at least one AKLT-entangled pair is $S = 2$. From this it follows trivially that H_K annihilates $|X\rangle$ and $|Y\rangle$; moreover, since H_K is positive semidefinite, this proves that they are ground states.

It is only slightly more difficult to see that any other state constructed as a direct product of AKLT-loop states has positive energy: since each site can be AKLT entangled with at most two other sites, and since there are four elementary triangles per site, in any zero energy state exactly two of the sites must be AKLT-entangled, and each entangled pair must form an edge of four distinct elementary triangles. The two states $|X\rangle$ and $|Y\rangle$ are the only ones that satisfy this constraint. For instance, if the blue bonds in Fig. 4 make a turn, an elementary triangle with its vertex at the corner of the turn will not contain any AKLT-entangled pair. While we do not have a general proof that no more complex ground states exist, explicit finite cluster diagonalization (up to system size 4×4) suggest that there are none.

From the known properties of AKLT states,^{21,22} it follows immediately that $|X\rangle$ and $|Y\rangle$ are gapped PM states with exponentially falling spin-spin correlations which break crystal rotation symmetry: $G_X(\vec{R}_{ij}) \equiv \langle X | \mathbf{S}_i \cdot \mathbf{S}_j | X \rangle = 9 \cos(\vec{R}_{ij} \cdot \vec{Q}_N) \delta(\vec{R}_{ij} \cdot \hat{y}) e^{-|\vec{R}_{ij} \cdot \hat{x}|/\xi_0}$ with $\vec{Q}_N = \pi(\hat{x} + \hat{y})$ and $\xi_0 = 1/\ln(3)$ in units in which the lattice constant is 1. The gap implies that the nematic PM phase is perturbatively stable. However, the asymptotic form of G is non-generic – this reflects the fact that H_K lies on a “disorder line²³” where, although there

is no associated thermodynamic non-analyticity, the oscillatory character of the short-range order changes.

Turning to less “reverse engineered” models, we discuss the very interesting numerical (density matrix renormalization group) study by Jiang *et al.*²⁴ of the spin-1 version of the $J_1 - J_2$ model in equation (1). They found that as a function of J_2/J_1 there is an intermediate paramagnetic phase (characterized by gapped $S = 1$ excitations) between the Néel and stripe ordered phases [see Fig. 3(c)]. Moreover the Néel and stripe order parameters vanish continuously as J_2/J_1 approaches the respective critical values from the magnetically ordered side (see Fig. 4 of Ref.²⁴). In the supplementary information we perform exact diagonalization on small lattices and demonstrate the adiabatic connectivity of the ground-state phases of H_K (equation (2)) and the $J_1 - J_2$ model when J_2/J_1 falls within the PM regime. In addition we compare the excitations in different spin and momentum sectors.

To obtain an analytic understanding of the nematic quantum PM phase, we consider a field theory description valid in the neighborhood of a continuous or weakly first order quantum phase transition from the Néel phase to a nematic PM phase. Because the unbroken symmetries of the Néel and nematic PM phases do not have a subgroup relationship, classical Landau theory would imply that such a continuous phase transition is forbidden. However as pointed out in Ref.²⁵, when the topological defects of one order carry the quantum number of the other order a continuous transition becomes possible.

According to Ref.⁵, in the path integral describing the quantum fluctuations of the $S = 1$ Néel antiferromagnet in 2D, the weight associated with each field configuration is determined by the usual non-linear sigma model (analogous to the first term in equation (3)), but there is also an additional Berry’s phase factor. For a “charge” q_m monopole (which causes the skyrmion number to jump by q_m) centered on plaquette $\vec{\mathcal{R}}$ (which designates a point on the dual lattice) this phase factor (up to a global “gauge” ambiguity) is $\eta_{\vec{\mathcal{R}}} = e^{iq_m(\vec{Q}_N \cdot \vec{\mathcal{R}})}$. [see Fig. 1(c)]. Rotation by 90° about a lattice site transforms $\eta_{\vec{\mathcal{R}}} \rightarrow -\eta_{\vec{\mathcal{R}}}$ but keeps q_m invariant. So long as this symmetry is preserved, the Feynman amplitude of any field configuration with an odd q_m cancels that associated with the configuration rotated by 90° . As a result odd q_m monopoles cannot proliferate, although even q_m monopoles can. Consequently, states can be classified by a conserved skyrmion number parity $(-1)^{q_s}$. It turns out that the two-fold degeneracy associated with opposite skyrmion parity accounts for the two nematic ground states depicted in Fig.4. If we introduce a perturbation that breaks the crystal 90° rotation

symmetry, the absolute value of the Feynman amplitudes associated with monopoles sitting at the $+1$ and -1 locations in Fig. 1(c) do not need to be the same anymore, hence their Feynman amplitudes no longer cancel which means the odd q_m monopoles can proliferate rendering the PM state non-degenerate. This observation justifies identifying the two-fold degeneracy in the symmetric system with spontaneous breaking of 90° rotation symmetry.

In the following discussions we will use Euclidean space-time and denote the imaginary time as τ . Consider a 4-component real vector field of unit norm, $\hat{\Omega}(x, y, \tau) = (\mathbf{\Omega}, \Omega_4)$ with $|\hat{\Omega}|^2 = 1$, whose first three components, $\mathbf{\Omega}(x, y, \tau)$ are the Néel order parameter and Ω_4 is the Ising-like nematic order parameter. For example, for a spin model on a square lattice, we can take $\Omega_4(x_i, y_i, \tau) \propto \langle \mathbf{S}_i \cdot \mathbf{S}_{i+\hat{x}} - \mathbf{S}_i \cdot \mathbf{S}_{i+\hat{y}} \rangle$. The non-linear sigma model action we shall consider is

$$S = \int d^2x d\tau \left[\frac{1}{2g} |\partial_\mu \hat{\Omega}|^2 + V(\Omega_4^2) \right] + i \frac{\Theta}{2\pi^2} \int d^2x d\tau \epsilon^{abcd} \Omega_a \partial_x \Omega_b \partial_y \Omega_c \partial_\tau \Omega_d, \quad (3)$$

where $\Theta = \pi$. This field theory has been introduced in Ref.²⁶ and Ref.²⁷ which discuss the effects of topological terms on the spectrum and phases of non-linear sigma models. For our purposes a derivation of equation (3) is given in the supplementary information. Note that this particular topological term is possible only in spatial dimension $d = 2$ with a $N = 4$ component order parameter. Here V is an anisotropy term that favors the first three components of $\hat{\Omega}$, (for example $V = \Delta[\Omega_4]^2$), hence equation (3) has $O(3) \times Z_2$ symmetry. Consider a monopole configuration centered on the origin, $(x, y, \tau) = (0, 0, 0)$. Because of the anisotropy term, $\hat{\Omega}$ on a two-sphere (S^2) in space-time far away from the center of the monopole is largely constrained to lie in the space spanned by the first three components of $\hat{\Omega}$, *i.e.* $\hat{\Omega} \approx (\hat{n}, 0)$. Topologically the configurations of \hat{n} on the two-sphere are classified by the skyrmion number which, in this case, is equal to the monopole charge q_m . However such far field configuration can be compatible with two different Ω_4 orientations in the monopole core. Consider the following configurations which reduce to the same $q_m = 1$ configuration in \hat{n} far from monopole the center

$$\hat{\Omega}^{(\pm)}(x, y, \rho) = (\sin \phi_\pm(\rho) \hat{n}(x, y, \rho), \cos \phi_\pm(\rho)), \quad (4)$$

where $\rho = \sqrt{x^2 + y^2 + \tau^2}/R$, $\phi_+(\rho) = \frac{\pi}{2} \tanh(\rho)$, and $\phi_-(\rho) = \pi(1 - \frac{1}{2} \tanh(\rho))$. Here R is the size of the ‘‘monopole core’’. $\hat{\Omega}^{(\pm)}$ both describe $q_m = 1$ monopoles but with $\hat{\Omega} = (\mathbf{0}, \pm 1)$ in the monopole core. It is straightforward to show that

$\exp\{i\frac{\Theta}{2\pi^2} \int d^2x d\tau \epsilon^{abcd} \Omega_a \partial_x \Omega_b \partial_y \Omega_c \partial_\tau \Omega_d\} = e^{\pm i\pi/2} = \pm i$ for these two types of monopole. A similar discussion holds for the $q_m = -1$ monopole. It is easy to generalize the above argument to $q_m = 2$ monopoles and obtain the corresponding phase factors $e^{\pm i\pi} = -1$. A consequence of the Z_2 (nematic) symmetry is that the Feynman amplitudes of the two monopoles described above have the same absolute values.

These monopoles represent events (as a function of imaginary time) at which the skyrmion number changes. We can thus think of the quantum disordered phase as an interacting fluid of skyrmions and anti-skyrmions. Because of the destructive interference between the two types of $q_m = 1$ monopoles discussed above, events in which the skyrmion number changes by one are forbidden – the net skyrmion number is thus conserved modulo 2 and the Hilbert space breaks into an even and an odd sector. Since the stiffness constant $1/g$ renormalizes to zero in the quantum disordered state and since there is a non-zero (possibly small) density of skyrmions and anti-skyrmions, the ground-state energy in these two sectors should be equal in the thermodynamic limit. This is the ground-state degeneracy associated with the breaking of C_4 symmetry to C_2 . In the supplementary information we discuss the effects of an explicit $C_4 \rightarrow C_2$ symmetry breaking field.

One can also arrive at the PM phase in Fig. 3(c) from the stripe ordered side by proliferating the monopole of the stripe order parameter. Generalizing the calculation of Ref.⁵ we find the Berry’s phase factor associated with the stripe monopole is trivial. Consequently the charge ± 1 monopole can proliferate rendering the resulting quantum disordered state non-degenerate. Here, because the symmetries of the two phases have subgroup relationship, a continuous transition is allowed in the Landau theory. We expect such transition to be in the $O(3)$ universality class.

Our key theoretical conclusion is that for a spin-1 model on a square lattice, any “intermediate” quantum disordered phase between the Néel and stripe ordered magnetic phases is likely to be a nematic PM. This is consistent with the numerical evidence for the $J_1 - J_2$ model [equation (1)]. Because the nematic quantum PM phase straddles closely between the Neel and nematic phases, we expect it to have low-lying spin excitations near both momenta $(\pi, 0)$ and (π, π) . The nematic order considered here might be thought of as “vestigial” order²⁸ left behind when quantum fluctuations have restored spin-rotational symmetry.

Before speculating on the relevance of these results to the interesting case of FeSe, it is necessary to comment on the effects of itinerant carriers. ARPES and STM experiments

show very small electron and hole pockets for FeSe^{13,14,29} and at the same time quantum oscillation associated with these tiny pockets are seen^{13,30}. Because the latter experiment has very stringent requirement on the long life time of the quasiparticles we take it as an indication that the coupling between the itinerant carriers and the local moments is weak. This phase with decoupled magnetic and itinerant carrier degrees of freedom is analogous to the antiferromagnetic metal phase in heavy fermion systems. However due to the itinerant carriers the nematic phase can no longer be characterized as having a spin-gap, and close enough to criticality, the universality class of the quantum critical point is likely to be altered. In addition, FeSe is at best “quasi-2D,” which is to say that it is ultimately three dimensional, and this, too, will alter the nature of the phase transitions, but not necessarily affect the sequence of ordered phases.

Since the iron-based superconductors involve multiple $3d$ orbitals it has been long suspected that orbital ordering is the cause of nematicity. Although we focus on the nematicity caused by frustrated magnetism, we do not intend to imply that orbital degrees of freedom play no role at all. As is well known regardless of the driving mechanism the nematic order parameter induces orbital splitting and lattice distortion. Therefore cooperative effect involving many different degrees of freedom can well be necessary to describe the system behavior quantitatively. In addition the so far ignored spin orbit coupling is ultimately necessary for the nematicity in the magnetic degrees of freedom to induce the band splitting observed by ARPES and anisotropic magnetic susceptibility observed by NMR..etc.

With these caveats, the present results suggest that it may be possible to view the nematic phase in the FeSe as being driven primarily by frustrated magnetism. The fact that the underlying nematic quantum PM is gapped implies that there need not be any enhancement of the low energy magnetic fluctuations associated with the proximity of stripe long range order of the sort that has been detected by NMR in other Fe-based materials. Recent neutron scattering experiments³¹ show relatively short-range magnetic correlations but with reasonably large intensity (*i.e.* with substantial magnitudes of the fluctuating moments) at the stripe ordering wavevector at low energies. Consequently, the lack of any strong evidence of slow magnetic fluctuations in NMR²⁰ and the short-range of the magnetic correlations seen in neutron scattering appear to be entirely consistent with a magnetic origin of nematicity. As discussed previously we expect the nematic PM phase to also exhibit relatively low energy spin excitations at the Neel ordering wavevector. The nematic quantum PM state

consists of a stacking of spontaneously formed spin-1 AF chains. It can be viewed as a “weak” symmetry protected topological state. A potentially testable consequence of this observation is that gapless spin 1/2 excitations can arise on certain surfaces and domain boundaries. In addition we expect nonmagnetic impurities to cut the chain and induce low lying spin excitations in the PM gap. This can be detected by electron spin resonance in a manner analogous to that done for spin-1 chains³². Further experimental studies of nematic order and fluctuations in these materials – including elasto-resistance, nuclear quadrupole resonance, and Raman scattering studies – as well more complete neutron scattering studies of the magnetic fluctuations would clearly be helpful.

Finally after the submission of our paper, related theoretical studies appeared^{33,34} including one based on an itinerant electron picture of the nematicity in FeSe³⁵.

Acknowledgements: We thank Hongchen Jiang and Tao Xiang for useful discussions. FW was supported by National Key Basic Research Program of China (Grant No. 2014CB920902) and National Science Foundation of China (Grant No. 11374018). SAK was supported in part by the U.S. Department of Energy, Office of Science, Basic Energy Sciences, Materials Sciences and Engineering Division, grant DE-AC02-76SF00515 at Stanford. DHL was supported by the U.S. Department of Energy, Office of Science, Basic Energy Sciences, Materials Sciences and Engineering Division, grant DE-AC02-05CH11231. DHL and SAK would like to thank KITP for hospitality, supported in part by the National Science Foundation under Grant No. NSF PHY11-25915, where the collaboration started.

The Spin-1 Néel-Nematic Transition as a double Spin-1/2 Néel-VBS Transition

It has been proposed that a Landau-forbidden continuous quantum phase transition between Néel order and valence bond solid can happen in spin-1/2 systems on square lattice. This transition can be described by a non-linear sigma model (NL σ M) with a Wess-Zumino-Witten(WZW) term and certain anisotropy terms^{36,37}. The action of this model reads

$$S_{\frac{1}{2}}[\hat{\phi}] = S_{O(3)\times C_{4v}}[\hat{\phi}] - 2\pi i \frac{3}{8\pi^2} \int du d^2x d\tau \epsilon^{abcdf} \phi_a \partial_x \phi_b \partial_y \phi_c \partial_\tau \phi_d \partial_u \phi_f. \quad (5)$$

Here the 5-component “superspin” $\hat{\phi} \propto (n_x, n_y, n_z, v_x, v_y)$ consists of the Néel order parameters $\mathbf{n} = (n_x, n_y, n_z) \sim (-1)^{x+y} \mathbf{S}_{(x,y)}$, and the two columnar VBS order parameters

$\mathbf{v} = (v_x, v_y)$ where

$$v_x \sim (-1)^x (\mathbf{S}_{(x,y)} \cdot \mathbf{S}_{(x+1,y)} - \mathbf{S}_{(x,y)} \cdot \mathbf{S}_{(x-1,y)}), \quad (6a)$$

$$v_y \sim (-1)^y (\mathbf{S}_{(x,y)} \cdot \mathbf{S}_{(x,y+1)} - \mathbf{S}_{(x,y)} \cdot \mathbf{S}_{(x,y-1)}). \quad (6b)$$

u is the auxiliary dimension for defining the WZW term. $S_{O(3) \times C_{4v}}$ is the non-topological part of the non-linear sigma model action with $O(3) \times C_{4v}$ symmetry. This action includes the stiffness terms such as $\int d^2x d\tau \left(\frac{1}{2g_n} |\partial_\mu \mathbf{n}|^2 + \frac{1}{2g_v} |\partial_\mu \mathbf{v}|^2 \right)$. In addition it contains anisotropy terms that favor the Néel order parameters over the VBS order parameters. Moreover, among the VBS order parameters there are terms that favor the columnar VBS over the plaquette VBS order. Examples of such anisotropy terms include $\Delta \cdot (\phi_4^2 + \phi_5^2)$ (where $\Delta > 0$) and $U \cdot (\phi_4^2 - \phi_5^2)^2$ (where $U < 0$). In particular, $\Delta > 0$ insures that the low energy physics is described by the fluctuations of the Néel order parameters.

Spin-1 can be viewed as two spin-1/2s coupled by strong ferromagnetic(FM) interaction. We thus consider two copies of the action equation (5) labeled by superscripts ⁽¹⁾ and ⁽²⁾,

$$S_1[\hat{\phi}^{(1)}, \hat{\phi}^{(2)}] = S_{\frac{1}{2}}[\hat{\phi}^{(1)}] + S_{\frac{1}{2}}[\hat{\phi}^{(2)}] + \int d^2x d\tau (J_n \mathbf{n}^{(1)} \cdot \mathbf{n}^{(2)} + J_v \mathbf{v}^{(1)} \cdot \mathbf{v}^{(2)}). \quad (7)$$

We assume ‘‘FM’’ coupling between the Néel order parameters ($J_n < 0$) and ‘‘AFM’’ coupling between the VBS order parameters ($J_v > 0$) so that the low energy configurations have $\mathbf{n}^{(1)} = \mathbf{n}^{(2)} \equiv \mathbf{n}$ and $\mathbf{v}^{(1)} = -\mathbf{v}^{(2)} \equiv \mathbf{v}$. The action in terms of $\hat{\phi} = (\mathbf{n}, \mathbf{v})$ will be similar to equation (5) but with a *doubled* WZW term.

Note however $\mathbf{v} = \frac{1}{2}(\mathbf{v}^{(1)} - \mathbf{v}^{(2)})$ cannot be directly measured in spin-1 systems, because all physical observables must be symmetric with respect to exchange of the two spin-1/2 moments. Define two physical order parameters,

$$v'_1 = -\frac{v_x^{(1)}v_x^{(2)} - v_y^{(1)}v_y^{(2)}}{\sqrt{v_x^2 + v_y^2}}, \quad v'_2 = -\frac{v_x^{(1)}v_y^{(2)} + v_x^{(2)}v_y^{(1)}}{\sqrt{v_x^2 + v_y^2}}. \quad (8)$$

v'_1 carries lattice momentum $(0, 0)$, belongs to the B_1 representation of C_{4v} (changes sign under 4-fold rotation, but has no sign change under principal axis reflection), and corresponds to the nematic order parameter Ω_4 defined in the main text (for example, the parent Hamiltonian ground state $|X\rangle$ in the main text corresponds to $v_x^{(1)} = -v_x^{(2)} \neq 0$ and $v_y^{(1)} = -v_y^{(2)} = 0$ and thus $v'_1 > 0$). v'_2 has lattice momentum (π, π) , is the B_2 representation of C_{4v} (changes sign under both 4-fold rotation and principal axis reflection around a lattice site), and corresponds to certain superpositions of plaquette valence bond solid

order (for example, $v'_2 < 0$ may correspond to either $v_x^{(1)} = v_y^{(2)} > 0$ with plaquette singlets centered at $(2x + 1/2, 2y + 1/2)$, or $v_y^{(1)} = v_x^{(2)} < 0$ with plaquette singlets centered at $(2x - 1/2, 2y - 1/2)$ for integer x, y). If we parametrize \mathbf{v} by $(v_x, v_y) = (v \cos \theta, v \sin \theta)$, then $\mathbf{v}' = (v'_1, v'_2) = (v \cos 2\theta, v \sin 2\theta)$. Note that

$$\begin{aligned} v'_1 \partial_\mu v'_2 - v'_2 \partial_\mu v'_1 &= 2v^2 \partial_\mu \theta = 2(v_x \partial_\mu v_y - v_y \partial_\mu v_x), \\ \partial_\mu v'_1 \partial_\nu v'_2 - \partial_\mu v'_2 \partial_\nu v'_1 &= 2v(\partial_\mu v \partial_\nu \theta - \partial_\mu \theta \partial_\nu v) = 2(\partial_\mu v_x \partial_\nu v_y - \partial_\mu v_y \partial_\nu v_x). \end{aligned}$$

Therefore the WZW term in action S_1 in terms of $\hat{\phi}' \propto (\mathbf{n}, \mathbf{v}') = (n_x, n_y, n_z, v'_1, v'_2)$ has a *halved* coefficient compared to that in terms of (\mathbf{n}, \mathbf{v}) . The action then becomes

$$S_1[\hat{\phi}^{(1)}, \hat{\phi}^{(2)}] \sim S_1[\hat{\phi}'] = S_{O(3) \times Z_2 \times Z_2}[\hat{\phi}'] - 2\pi i \frac{3}{8\pi^2} \int d^2x d\tau \epsilon^{abcdf} \phi'_a \partial_x \phi'_b \partial_y \phi'_c \partial_\tau \phi'_d \partial_u \phi'_f. \quad (9)$$

The action $S_{O(3) \times Z_2 \times Z_2}[\hat{\phi}']$ is derived from $S_{O(3) \times C_{4v}}[\hat{\phi}]$ while taking equation (8) into account. It has $O(3) \times Z_2 \times Z_2$ anisotropy induced by the additional anisotropy terms such as $\Delta_4 \cdot \phi_4'^2$ and $\Delta_5 \cdot \phi_5'^2$ where $\Delta_{4,5} > 0$.

Assume $\Delta_5 \gg \Delta_4 > 0$. Consider the configuration

$$\hat{\phi}'(u, x, y, \tau) = \left(\hat{\Omega}(x, y, \tau) \sin(u), \cos(u) \right),$$

where $\hat{\Omega}$ is the 4-component real vector field in Eq. (6) of the main text. When $u = 0$ this is a uniform space-time configuration, and when $u = \pi/2$ this will be a low energy space-time configuration with $\phi_5' = 0$. Integrate over u from 0 to $\pi/2$, the WZW term becomes

$$\begin{aligned} & - 2\pi i \frac{3}{8\pi^2} \int d^2x d\tau \epsilon^{abcd} \Omega_a \partial_x \Omega_b \partial_y \Omega_c \partial_\tau \Omega_d \cdot \int_0^{\pi/2} du (-\sin^5 u - \sin^3 u \cos^2 u) \\ &= - 2\pi i \frac{3}{8\pi^2} \int d^2x d\tau \epsilon^{abcd} \Omega_a \partial_x \Omega_b \partial_y \Omega_c \partial_\tau \Omega_d \cdot (-2/3) \\ &= i \frac{\pi}{2\pi^2} \int d^2x d\tau \epsilon^{abcd} \Omega_a \partial_x \Omega_b \partial_y \Omega_c \partial_\tau \Omega_d \end{aligned}$$

In the above the $(-\sin^5 u)$ and $(-\sin^3 u \cos^2 u)$ terms are respectively from $abcdf = abcd5$ and $abcdf = 5bcda$ terms in the WZW model (terms with index “5” at other positions vanish). This result is exactly the Θ -term in equation (6) of the main text with $\Theta = \pi$. Thus the final effective action is given by equation (6) of the main text. (Note that due to the anisotropy term $V(\Omega_4^2)$ the stiffness constant for the first three components of $\hat{\Omega}$ will be different from that of Ω_4 at low energies and long wavelengths.)

In the above discussion we have made the assumptions that $J_n < 0$ and $J_v > 0$ in equation (7), and $\Delta_5 \gg \Delta_4 > 0$ in equation (9). Here we briefly comment on several other possibilities.

(i). If $J_n < 0$ and $J_v < 0$, the low energy configurations in equation (7) will be $\mathbf{n}^{(1)} = \mathbf{n}^{(2)} \equiv \mathbf{n}$ and $\mathbf{v}^{(1)} = \mathbf{v}^{(2)} \equiv \mathbf{v}$, this theory would describe the phase transition from Néel AFM order (\mathbf{n}) to columnar VBS order (\mathbf{v}) with a WZW term similar to that of equation (5) but with doubled coefficient.

(ii). If $J_n > 0$, the low energy configurations in equation (7) would have $\mathbf{n}^{(1)} = -\mathbf{n}^{(2)} \equiv \mathbf{n}$, then \mathbf{n} is the director of the uniaxial spin-nematic order (uniaxial spin-nematic states have $|\mathbf{n} \cdot \mathbf{S} = 0\rangle$). This theory would describe the phase transition between ferro-spin-nematic order and columnar VBS order (if $J_v < 0$) or a nematic quantum paramagnet (if $J_v > 0$). However the WZW term would be absent, so we expect this phase transition to be of first-order.

(iii). If $J_n < 0$ and $J_v > 0$ as we assumed in equation (7), but $\Delta_4 \gg \Delta_5 > 0$ in equation (9). This theory would describe the phase transition between Néel order and plaquette VBS order.

The effects of explicit $C_4 \rightarrow C_2$ symmetry breaking field.

To explicitly break the C_4 symmetry to C_2 , we can introduce a Z_2 “Zeeman” field

$$S \rightarrow S + h \int d^2x d\tau \Omega_4(x, y, \tau), \quad (10)$$

which breaks the degeneracy between the two types of monopole in Eq.(7) of the main text, making the absolute value of the Feynman amplitude associated them different – hence they do not cancel. Now tunneling events involving unit changes in the skyrmion number are allowed, which causes mixing between the even and odd skyrmion sectors which lifts the ground-state degeneracy.

Here we propose the renormalization group flow diagram [Fig. 5] of equation (10). Along the vertical axis at $h = 0$ there is a continuous (Landau-forbidden), or weakly first order, phase transition between the small g Néel state and the large g two-fold degenerate nematic PM phase. This is supported by Fig. 4 of Ref.²⁴. Along the axis where the absolute value of h is large the transition from the anisotropic Néel state (where there is Néel long-range

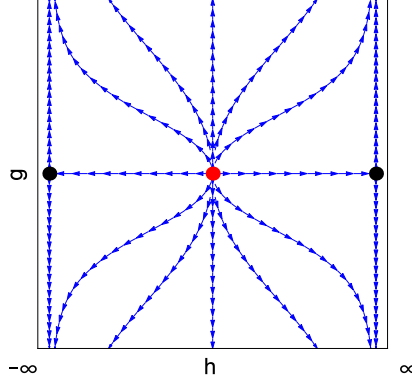


FIG. 5: **The renormalization group flow diagram of equation (10). The fixed points value of g in this figure are all $O(1)$.** The proposed renormalization group flow diagram of equation (10). Along the $h = 0$ axis the red critical point separates the small g Néel ordered state from the large g nematic paramagnetic state. Such transition if continuous will be an example of Landau-forbidden transition. The blue critical point separates the anisotropic Néel state (a state with Néel long range order but $\langle \mathbf{S}_i \cdot \mathbf{S}_{i+\hat{x}} \rangle \neq \langle \mathbf{S}_i \cdot \mathbf{S}_{i+\hat{y}} \rangle$) and the anisotropic paramagnetic phase. Such phase transitions should belong to the $O(3)$ universality class.

order but $\langle \mathbf{S}_i \cdot \mathbf{S}_{i+\hat{x}} \rangle \neq \langle \mathbf{S}_i \cdot \mathbf{S}_{i+\hat{y}} \rangle$) into the PM state [this transition happens at the lower boundary of the diagonal strip in Fig. 6 discussed below] is in the usual $O(3)$ universality class. In the large g region of Fig. 5, where the system remains PM, tuning h from negative to positive encounters a first order phase transition at $h = 0$ while maintaining a nonzero $S = 1$ gap.

Returning to the numerical results of Ref.²⁴, note that Jiang *et al.* did study the effect of explicit rotation symmetry breaking on their results by introducing anisotropy in the NN exchange constants in the x and y directions, so that $J_{1y} > J_{1x}$. They found for $0 \leq h \equiv (J_{1y} - J_{1x})/J_{1y} \leq 1$ there is always (for some range of J_2/J_{1y}) an intermediate PM phase between the Néel and stripe ordered phases [see Fig. 6 for a schematic illustration]. Within this PM phase, they found no evidence of a phase transition, suggesting that it is all one phase. Remarkably it is found that not only does this PM phase survive for $0.525 \lesssim J_2/J_1 \lesssim 0.555$ in the isotropic limit $h \rightarrow 0$, but it also includes the case $J_2 = 0$ and $h = 1$, where the system consists of a decoupled array of spin-1 chains. As it is independently known that the spin-1 AF chain is in the same phase as the spin-1 AKLT

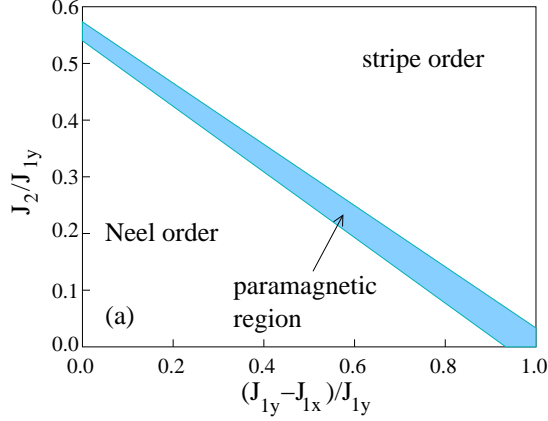


FIG. 6: **The phase diagram of the J_1 - J_2 model, Eq. 1 of the main text.** A schematic reproduction of the phase diagram reported in Ref.²⁴. The line of $J_{1y} - J_{1x} = 0$ shows the phase diagram for the J_1 - J_2 model, Eq. 1 of the main text, with fourfold rotation symmetry.

chain, this observation nicely connects the results of the $J_1 - J_2$ model to those obtained for H_K .

Finally, the other interesting scenario²⁷, namely, the gapless state of Eq. (6) in main text at $\Theta = \pi$ can be viewed as the critical state between two different SPTs (one at $\Theta = 0$ and the other $\Theta = 2\pi$). Presumably such critical state can be obtained by proliferating the domain walls in the nematic order parameter in our nematic PM phase. Further works are definitely deserved.

Exact diagonalization results for the the $S = 1$ J_1 - J_2 model

Exact diagonalization was performed on 4×4 square lattices with periodic boundary conditions for the spin-1 J_1 - J_2 antiferromagnetic Heisenberg model

$$H = J_1 \sum_{\langle ij \rangle} \mathbf{S}_i \cdot \mathbf{S}_j + J_2 \sum_{\langle\langle jk \rangle\rangle} \mathbf{S}_j \cdot \mathbf{S}_k. \quad (11)$$

The spin singlet and spin triplet gaps at momenta $\vec{q} = (\pi, 0)$ and (π, π) are presented for different values of J_2/J_1 in Fig. 7 The global spin-1 gap is given by the minimum of the blue and dashed black curves. As a result it exhibits a kink consistent with that reported in

Ref.²⁴. What is noteworthy are (1) the spin-0 gap plunges in the range of J_2/J_1 where the nematic quantum PM state is expected. This presumably reflects the small splitting (due to quantum tunneling) between the two states that would be degenerate in the thermodynamic limit. (2) As the $(\pi, 0)$ triplet gap vanishes as J_2/J_1 approaches the PM to stripe phase boundary, the (π, π) triplet gap steadily increases. The reverse is true as J_2/J_1 approaches the PM to Neel phase boundary. That within the PM regime, the $\Delta_{S=1}(\pi, \pi)$ is small compared to $\Delta_{S=1}(\pi, 0)$ on the small J_2/J_1 and large on the large J_2/J_1 side suggests the existence of two closeby quantum phase transitions plays a key role in the physics.

The ground state fidelity susceptibility³⁸ is presented in Fig. 8. This quantity displays a clear peak providing strong evidence of a quantum phase transition(s) within $0.5 < J_2/J_1 < 0.6$, even on such a small lattice. This result could be interpreted as indicating a single strongly first-order transition (which is inconsistent with the result of Ref.²⁴). Alternatively it can be taken as evidence of the existence of two (continuous) transitions (favored by the result of Ref.²⁴).

Exact diagonalization results for a model interpolating between the parent Hamiltonian and J_1 - J_2 model

We consider a model which interpolates between the parent Hamiltonian H_K in Eq. (2) of the main text and the J_1 - J_2 Heisenberg model,

$$\begin{aligned}
 H_\lambda &= \lambda \cdot \frac{15 J_1}{4 K} \cdot H_K + (1 - \lambda) \cdot (J_1 \sum_{\langle ij \rangle} \mathbf{S}_i \cdot \mathbf{S}_j + J_2 \sum_{\langle\langle ij \rangle\rangle} \mathbf{S}_i \cdot \mathbf{S}_j) \\
 &= J_1 \sum_{\langle ij \rangle} \mathbf{S}_i \cdot \mathbf{S}_j + [J_2 + \lambda (J_1/2 - J_2)] \sum_{\langle\langle ij \rangle\rangle} \mathbf{S}_i \cdot \mathbf{S}_j + \lambda \cdot (\text{higher order terms}),
 \end{aligned} \tag{12}$$

where the “higher order terms” contain those terms involving 4 or 6 spin operators. This model becomes the parent Hamiltonian $\frac{15 J_1}{4 K} \cdot H_K$ at $\lambda = 1$, and the J_1 - J_2 Heisenberg model at $\lambda = 0$. We study the behavior of this model for three different J_2/J_1 values,

- $J_2/J_1 = 0$: the J_1 - J_2 Heisenberg model in this case should exhibit Néel order. The results for the interpolating model are shown in Fig. 9 and Fig. 10. In particular the

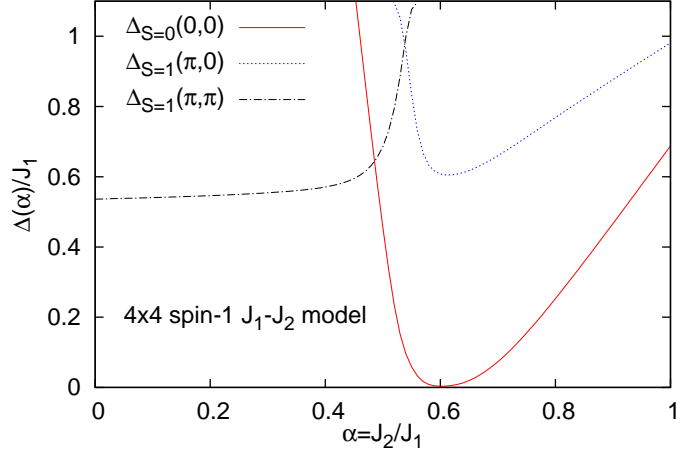


FIG. 7: The global singlet ($\Delta_{S=0}$) gap and the triplet ($\Delta_{S=1}$) gaps at momenta $\vec{q} = (\pi, 0)$ and (π, π) for the spin-1 J_1 - J_2 model on 4×4 lattice obtained by exact diagonalization. The global triplet gap result is the minimum of the blue and black dashed curves. It exhibits a sharp kink consistent with the DMRG results of Ref.²⁴. Due to the quantum tunneling between the two degenerate nematic PM states on finite lattices, one expects a unique singlet ground state and a small gap for the singlet excitations. The unique ground state for a given $\alpha = J_2/J_1$ is a spin singlet and has lattice momentum $(0, 0)$. The singlet gap is small when J_2/J_1 falls in the region where the nematic PM state exists (it nearly vanishes around $\alpha = 0.6$ where $\Delta_{S=0}(\alpha = 0.6) = 0.0033J_1$). Moreover the lowest energy singlet excited state has lattice momentum $(0, 0)$, suggesting no translation symmetry breaking in the tentative nematic quantum PM state. The triplet gap has a cusp around $\alpha = 0.54$. The lowest energy $S = 1$ states for $\alpha < 0.54$ have lattice momentum (π, π) consistent with Néel order, and the lowest energy $S = 1$ states for $\alpha > 0.54$ have lattice momentum $(\pi, 0)$ or $(0, \pi)$ consistent with stripe antiferromagnetic order.

ground state fidelity susceptibility shown in Fig. 10 has a prominent peak at around $\lambda = 0.9$, suggesting a phase transition from nematic paramagnet at $\lambda = 1$ to Néel order at $\lambda = 0$.

- $J_2/J_1 = 0.54$: according to the DMRG result in Ref.²⁴, the J_1 - J_2 Heisenberg model in this case will be in PM phase. The results for the interpolating model are shown in

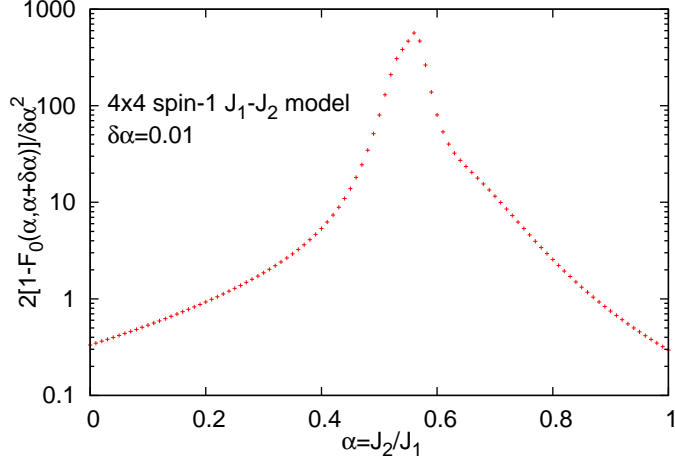


FIG. 8: Ground state fidelity susceptibility for the spin-1 J_1 - J_2 model on 4×4 lattice. The ground state fidelity $F_0(\alpha, \alpha + \delta\alpha) = |\langle \psi_0(\alpha + \delta\alpha) | \psi_0(\alpha) \rangle|$ is the overlap between ground states (ψ_0) at parameter α and $\alpha + \delta\alpha$. There is a sharp peak at around $\alpha = 0.56$.

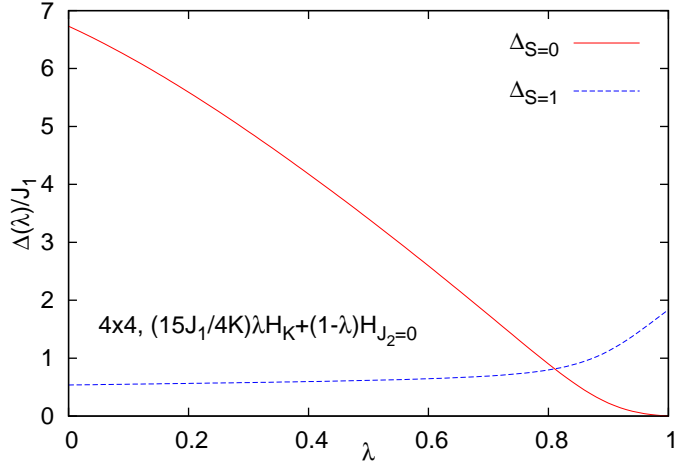


FIG. 9: Singlet ($\Delta_{S=0}$) and triplet ($\Delta_{S=1}$) gaps for the spin-1 interpolating model equation (12) with $J_2 = 0$ on 4×4 lattice.

Fig. 11 and Fig. 12. The ground state fidelity susceptibility shown in Fig. 12 has no peak, suggesting that the nonmagnetic phase at $\lambda = 0$ ($J_2/J_1 = 0.54$) is also a nematic paramagnet as the ground states of $\lambda = 1$ parent Hamiltonian.

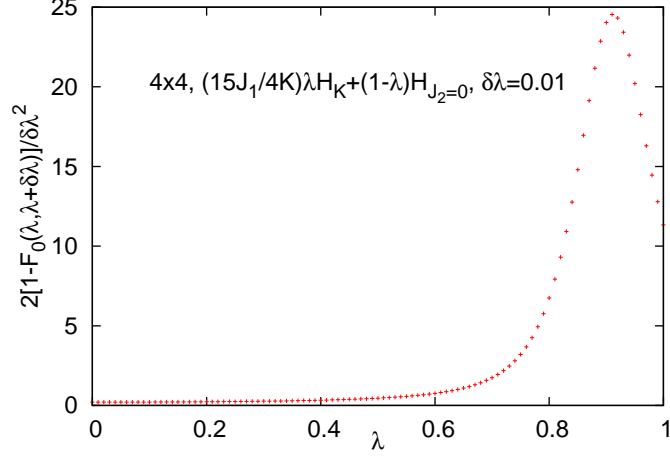


FIG. 10: Ground state fidelity susceptibility for the spin-1 interpolating model equation (12) with $J_2 = 0$ on 4×4 lattice. There is a peak at around $\lambda = 0.9$, suggesting that this marks the transition point of a nematic paramagnetic phase for $\lambda > 0.9$ to a Néel ordered state for $\lambda < 0.9$.

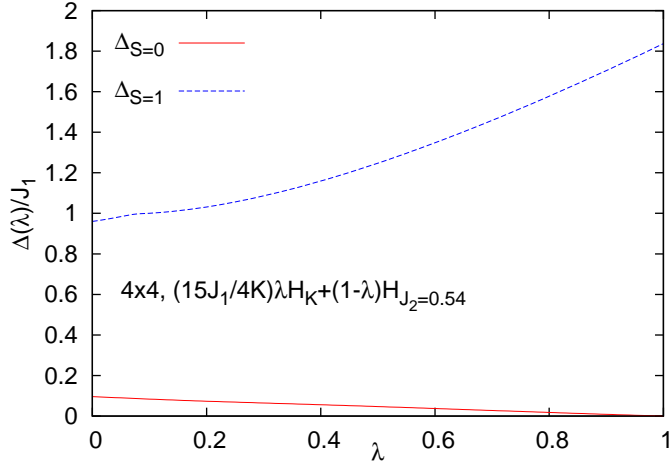


FIG. 11: Singlet ($\Delta_{S=0}$) and triplet ($\Delta_{S=1}$) gaps for the spin-1 interpolating model equation (12) with $J_2/J_1 = 0.54$ on 4×4 lattice. The singlet gap remains small, suggesting that the nematic paramagnet phase persists to J_1 - J_2 model limit ($\lambda = 0$).

- $J_2/J_1 = 1$: for this parameter choice the J_1 - J_2 Heisenberg model should be deep inside the stripe magnetic ordered phase. The results for the interpolating model are shown in Fig. 13 and Fig. 14. The ground state fidelity susceptibility shown in Fig. 14 has a prominent peak at around $\lambda = 0.8$, suggesting a phase transition from nematic paramagnet at $\lambda = 1$ to stripe order at $\lambda = 0$.

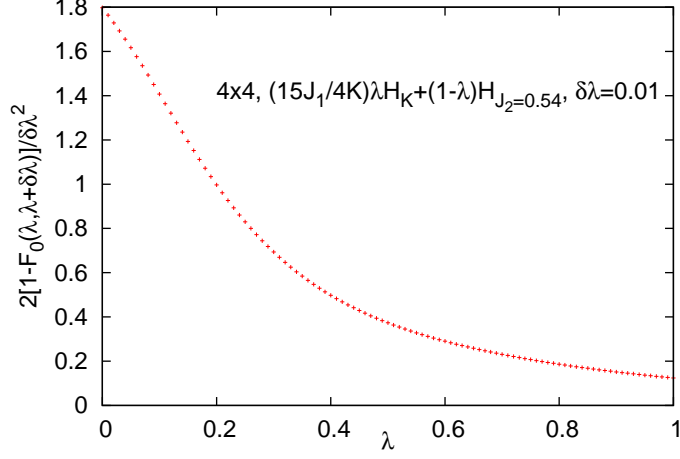


FIG. 12: Ground state fidelity susceptibility for the spin-1 interpolating model equation (12) with $J_2/J_1 = 0.54$ on 4×4 lattice. There is no peak, suggesting no phase transition from nematic paramagnet at $\lambda = 1$ to the nonmagnetic phase at $\lambda = 0$.

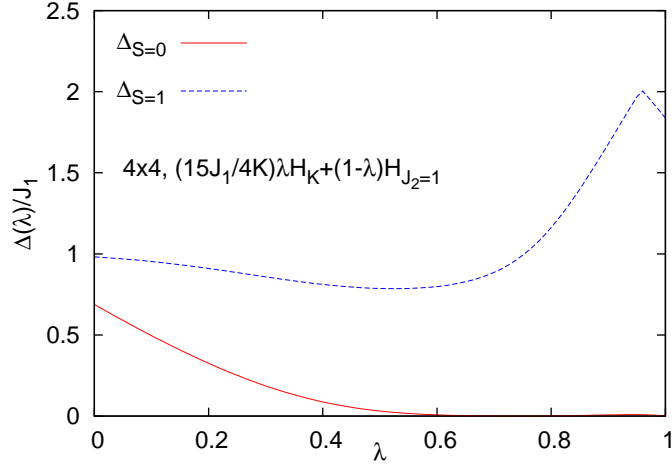


FIG. 13: Singlet ($\Delta_{S=0}$) and triplet ($\Delta_{S=1}$) gaps for the spin-1 interpolating model equation (12) with $J_2/J_1 = 1$ on 4×4 lattice. The singlet gap remains small for $\lambda > 0.8$, suggesting that the nematic paramagnet phase persists in this region.

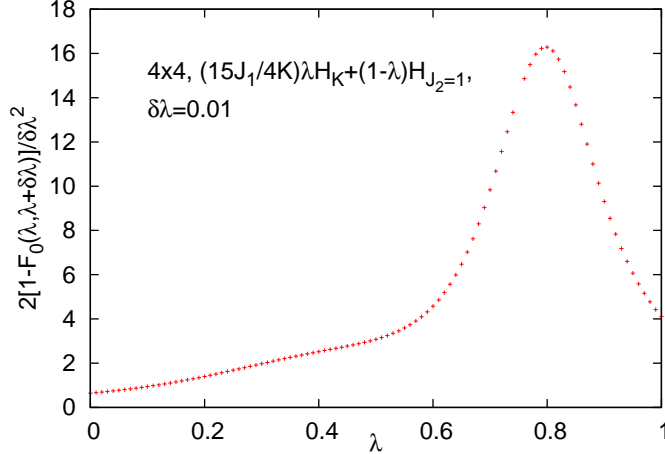


FIG. 14: Ground state fidelity susceptibility for the spin-1 interpolating model equation (12) with $J_2/J_1 = 1$ on 4×4 lattice. There is a peak at around $\lambda = 0.8$, that this marks the transition point of a nematic paramagnetic phase for $\lambda > 0.8$ to a stripe ordered state for $\lambda < 0.8$.

-
1. Anderson, P. W. The resonating valence bond state in La_2CuO_4 and superconductivity. *Science* **235**, 1196–1198 (1987).
 2. Figueirido, F. *et al.* Exact diagonalization of finite frustrated spin-(1/2) heisenberg models. *Phys. Rev. B* **41**, 4619–4632 (1990).
 3. Jiang, H.-C., Yao, H. & Balents, L. Spin liquid ground state of the spin- $\frac{1}{2}$ square J_1 - J_2 heisenberg model. *Phys. Rev. B* **86**, 024424 (2012).
 4. Gong, S.-S., Zhu, W., Sheng, D. N., Motrunich, O. I. & Fisher, M. P. A. Plaquette ordered phase and quantum phase diagram in the spin- $\frac{1}{2}$ J_1 - J_2 square heisenberg model. *Phys. Rev. Lett.* **113**, 027201 (2014).
 5. Haldane, F. D. M. $O(3)$ nonlinear σ model and the topological distinction between integer- and half-integer-spin antiferromagnets in two dimensions. *Phys. Rev. Lett.* **61**, 1029–1032 (1988).
 6. Read, N. & Sachdev, S. Valence-bond and spin-Peierls ground states of low-dimensional quantum antiferromagnets. *Phys. Rev. Lett.* **62**, 1694–1697 (1989).
 7. Qazilbash, M. M. *et al.* Electronic correlations in the iron pnictides. *Nat. Phys.* **5**, 674–650 (2009).
 8. Si, Q., Abrahams, E., Dai, J. & Zhu, J.-X. Correlation effects in the iron pnictides. *New*

- Journal of Physics* **11**, 045001 (2009).
9. Yin, Z. P., Haule, K. & Kotliar, G. Kinetic frustration and the nature of the magnetic and paramagnetic states in iron pnictides and iron chalcogenides. *Nat. Mater.* **10**, 932–935 (2011).
 10. Gretarsson, H. *et al.* Revealing the dual nature of magnetism in iron pnictides and iron chalcogenides using x-ray emission spectroscopy. *Phys. Rev. B* **84**, 100509 (2011).
 11. Maletz, J. *et al.* Unusual band renormalization in the simplest iron-based superconductor FeSe_{1-x}. *Phys. Rev. B* **89**, 220506 (2014).
 12. Nakayama, K. *et al.* Reconstruction of band structure induced by electronic nematicity in an FeSe superconductor. *Phys. Rev. Lett.* **113**, 237001 (2014).
 13. Watson, M. D. *et al.* Emergence of the nematic electronic state in FeSe. *Phys. Rev. B* **91**, 155106 (2015).
 14. Zhang, P. *et al.* Observation of two distinct d_{xz}/d_{yz} band splittings in FeSe. *Phys. Rev. B* **91**, 214503 (2015).
 15. Chu, J.-H., Kuo, H.-H., Analytis, J. G. & Fisher, I. R. Divergent nematic susceptibility in an iron arsenide superconductor. *Science* **337**, 710–712 (2012).
 16. Chandra, P., Coleman, P. & Larkin, A. Ising transition in frustrated heisenberg models. *Phys. Rev. Lett.* **64**, 88–91 (1990).
 17. Fang, C., Yao, H., Tsai, W.-F., Hu, J. & Kivelson, S. A. Theory of electron nematic order in LaFeAsO. *Phys. Rev. B* **77**, 224509 (2008).
 18. Xu, C., Müller, M. & Sachdev, S. Ising and spin orders in the iron-based superconductors. *Phys. Rev. B* **78**, 020501 (2008).
 19. Baek, S.-H. *et al.* Orbital-driven nematicity in FeSe. *Nat. Mater.* **14**, 210–214 (2015).
 20. Böhmer, A. E. *et al.* Origin of the tetragonal-to-orthorhombic (nematic) phase transition in FeSe: a combined thermodynamic and NMR study. *Phys. Rev. Lett.* **114**, 027001 (2015).
 21. Affleck, I., Kennedy, T., Lieb, E. H. & Tasaki, H. Rigorous results on valence-bond ground states in antiferromagnets. *Phys. Rev. Lett.* **59**, 799–802 (1987).
 22. Arovas, D. P., Auerbach, A. & Haldane, F. D. M. Extended heisenberg models of antiferromagnetism: Analogies to the fractional quantum hall effect. *Phys. Rev. Lett.* **60**, 531–534 (1988).
 23. Peschel, I. & Emery, V. Calculation of spin correlations in two-dimensional Ising systems from one-dimensional kinetic models. *Zeitschrift für Physik B Condensed Matter* **43**, 241–249

- (1981).
24. Jiang, H. C. *et al.* Phase diagram of the frustrated spatially-anisotropic $s = 1$ antiferromagnet on a square lattice. *Phys. Rev. B* **79**, 174409 (2009).
 25. Senthil, T., Vishwanath, A., Balents, L., Sachdev, S. & Fisher, M. P. A. Deconfined quantum critical points. *Science* **303**, 1490–1494 (2004).
 26. Abanov, A. & Wiegmann, P. Theta-terms in nonlinear sigma-models. *Nuclear Physics B* **570**, 685–698 (2000).
 27. Xu, C. & Ludwig, A. W. W. Nonperturbative effects of a topological theta term on principal chiral nonlinear sigma models in $2 + 1$ dimensions. *Phys. Rev. Lett.* **110**, 200405 (2013).
 28. Nie, L., Tarjus, G. & Kivelson, S. A. Quenched disorder and vestigial nematicity in the pseudogap regime of the cuprates. *Proc. Nat. Acad. Sci. USA* **111**, 7980–7985 (2014).
 29. Kasahara, S. *et al.* Field-induced superconducting phase of FeSe in the BCS-BEC cross-over. *Proc. Nat. Acad. Sci. USA* **111**, 16309–16313 (2014).
 30. Terashima, T. *et al.* Anomalous fermi surface in FeSe seen by Shubnikov-de Haas oscillation measurements. *Phys. Rev. B* **90**, 144517 (2014).
 31. Wang, Q. *et al.* Strong interplay between stripe spin fluctuations, nematicity and superconductivity in FeSe. *arXiv:1502.07544 (unpublished)* (2015).
 32. Glarum, S. H., Geschwind, S., Lee, K. M., Kaplan, M. L. & Michel, J. Observation of fractional spin $S=1/2$ on open ends of $S = 1$ linear antiferromagnetic chains: Nonmagnetic doping. *Phys. Rev. Lett.* **67**, 1614–1617 (1991).
 33. Glasbrenner, J. K., Mazin, I. I., Jeschke, H. O., Hirschfeld, P. J., Fernandes, R. M. & Valentí, R. Effect of magnetic frustration on nematicity and superconductivity in Fe chalcogenides. *Nat. Phys.* **11**, 953–958 (2015).
 34. Rong, Y. & Si, Q. Antiferroquadrupolar and Ising-nematic orders of a frustrated bilinear-biquadratic heisenberg model and implications for the magnetism of FeSe. *Phys. Rev. Lett.* **115**, 116401 (2015).
 35. Chubukov, A. V., Fernandes, R. M. & Schmalian, J. Origin of nematic order in FeSe. *Phys. Rev. B* **91**, 201105 (2015).
 36. Tanaka, A. & Hu, X. Many-body spin Berry phases emerging from the π -flux state: Competition between antiferromagnetism and the valence-bond-solid state. *Phys. Rev. Lett.* **95**, 036402 (2005).

37. Senthil, T. & Fisher, M. P. A. Competing orders, nonlinear sigma models, and topological terms in quantum magnets. *Phys. Rev. B* **74**, 064405 (2006).
38. Gu, S.-J. Fidelity approach to quantum phase transitions. *Int. J. Mod. Phys. B* **24**, 4371–4458 (2010).